Predictive model for local scour downstream of hydrokinetic turbines in erodible channels

Mirko Musa, Michael Heisel, and Michele Guala

Phys. Rev. Fluids **3**, 024606 — Published 22 February 2018

DOI: 10.1103/PhysRevFluids.3.024606

Predictive model for local scour downstream of hydrokinetic turbines in erodible channels

Mirko Musa,* Michael Heisel, and Michele Guala

Department of Civil, Environmental and Geo-Engineering,
University of Minnesota, Minneapolis, MN 55414, USA and
St. Anthony Falls Laboratory SAFL,
University of Minnesota, Minneapolis, MN 55414, USA

(Dated: February 2, 2018)

Abstract

A modeling framework is derived to predict the scour induced by Marine Hydrokinetic turbines (MHK) installed on fluvial or tidal erodible bed surfaces. Following recent advances in bridge scour formulation, the phenomenological theory of turbulence is applied to describe the flow structures that dictate the equilibrium scour depth condition at the turbine base. Using scaling arguments, we link the turbine operating conditions to the flow structures and scour depth through the drag force exerted by the device on the flow. The resulting theoretical model predicts scour depth using dimensionless parameters and considers two potential scenarios depending on the proximity of the turbine rotor to the erodible bed. The model is validated at the laboratory scale with experimental data comprising the two sediment mobility regimes (clear water and live bed), different turbine configurations, hydraulic settings, bed material compositions, and migrating bedform types. The present work provides future developers of flow energy conversion technologies with a physic-based predictive formula for local scour depth beneficial to feasibility studies and anchoring system design. A potential prototype-scale deployment in a large sandy river is also considered with our model to quantify how the expected scour depth varies as a function of the flow discharge and rotor diameter.

Keywords: renewable energy, turbulence, bridge pier, sediments, hydraulics

* mmusa@umn.edu

I. INTRODUCTION

In an effort to expand renewable energy extraction to tidal and fluvial environments, in-stream river turbines have been designed and tested in recent years both at the prototype scale [1–3] and at the laboratory scale in straight [4–6] and meandering channels [7]. The devices, usually referred to as marine hydrokinetic (MHK) turbines or current energy converters (CEC), have various shapes, efficiency, deployment strategies, and anchoring systems [see e.g. 8–12, among others].

Following the successful prototype deployment of Verdant Power in the East River in New York [1], we focus here on horizontal axis river turbines operating in open channel flows. The overall exploitable power is defined as $P = \frac{1}{2}\rho C_p(\pi D^2/4)U^3$, where the power coefficient C_p depends on the flow converter design and operating control. The representative mean velocity U impinging on the rotor D is usually taken as the undisturbed mean velocity at hub height. The available kinetic energy of the flow is limited by the relatively low river velocity, yet favored by the higher fluid density, as compared to wind energy. From the power estimate it is clear that more power can be extracted per device for larger rotor diameters D ($P \propto D^2$). Unlike traditional wind turbines in the atmospheric surface layer, the rotor diameter of hydrokinetic turbines in fluvial or tidal environments is constrained by the local flow depth. In addition, the rotating blades should not interact with any floating debris, logs, and ice, as well as boats and floaters. This upper limit condition essentially defines how much the device should be submerged for a range of flow discharges. The lower limit, i.e. the distance between the turbine bottom tip and the river bed, constrains both the rotor diameter and the hub height and is not trivial to optimize. For concrete artificial channels or bedrock fluvial systems, the wall boundary conditions are well defined and the only negative effect of the blade approaching the fixed bed is likely to be on the power coefficient [see, e.g. 13, on marine turbine wake evolution]. However, if the river bed is formed by erodible sediments, the problem becomes more complex due to the evolving boundary conditions affecting the structural integrity of the device in addition to its performance. On erodible beds, migrating bedforms make the bed elevation highly variable, while the rotating turbine is known to induce a local scour [5, 6]. The coupled bed fluctuations and local scour can potentially erode sediment around the device base and lead to the collapse of the supporting structure.

The scouring process around structures immersed in the flow, such as bridge piers, has been extensively studied in the past years and thoroughly covered in several text books [14–16]. However, it was recently demonstrated that the scour induced by hydrokinetic turbine is qualitatively and quantitatively different as compared to bridge pier scour [5]. Therefore, bridge pier models, of semi-empirical formulation [see, e.g. 17–23, among others], can not simply adapted for turbine scour. However, an elegant theoretical formulation was recently proposed and validated by [24], based on the framework developed by [25, 26] to interpret roughness effects in open channel flow and pipe flows.

The goals of this paper are to i) extend the theoretical model of [24] for bridge piers to provide a new modeling framework able to predict scour depth in the proximity of in-stream turbines under a range of flow and operating conditions, ii) validate the proposed turbine scour model using new experimental measurements and previously published experimental datasets, and iii) understand how the scouring mechanism may change depending on the distance of the rotor to the sediment bed. The rationale for this work is to provide an accessible analytical formulation as an alternative to high fidelity fluid dynamics simulations [27] for predicting the scour of MHK turbine deployments in sandy rivers.

In previous works, we have investigated experimentally the turbine scour under clear water (bed shear stress approaching the critical shear stress for sediment mobility) and live bed conditions (shear stress exceeding the critical value leading to sediment transport and bedform formation and migration). However, until now, we were not able to unambiguously define all the scaling quantities governing the scour mechanism. For example, the scour depth could potentially be normalized by the rotor diameter or by the depth of the river, with possible effects by the rotor location within the water column, the grain size, or the size of migrating bedforms. Because of the wide and complex parameter space, a theoretical description of the scour process based on the phenomenology of turbulence (in the terms discussed by [24–26]) is required to guide the functional dependencies of the model. This enables a rigorous scaling analysis to be formulated and extended to prototype-scale devices in natural rivers.

The turbine scour will be modeled here as a function of the turbine geometry and operating performance, incoming mean velocity and flow depth, sediment mobility regime, and bed material composition, thus comprising all the parameters relevant to MHK installations on erodible channels (Section II). Because of the varying vertical location of the turbine rotor, two modeling approaches are followed (Sections II A and II B). Experimental data (Section III) are used to independently validate the two model cases using time-averaged scour depth values (Section IV) and a probabilistic approach based on time-varying scour depths (Section IV D). The latter is introduced to quantify the scour depth variability observed under different migrating bedforms and hydraulic configurations, and compare such variability to the uncertainty associated with the model parameters. The scour model is further discussed and applied to a potential prototype-scale scenario (Section V). The main conclusions are provided in Section VI.

II. MODEL FRAMEWORK

We start from the mixed scaling approach originally proposed for rough wall open channel and pipe flow by [25, 26]. The approach relates the shear stress acting at the surface of the scour region in the proximity of the sediment grains exposed to the flow (see insert in Fig. 1) and estimated as the Reynolds stress $\tau = -\rho\overline{u'w'}$ for fully developed turbulence, to characteristic scales of the turbulent eddies. Following the argument by [25], the wall-normal fluctuations w' are dominated by eddies of the same size of the roughness asperities, represented here by sediment grains of diameter d. This specific eddy is the most energetic in the full range of turbulent eddies which can fit between nearby grains, and possibly mobilize them. In contrast, the longitudinal fluctuations u' scale with the energy containing eddies of the flow, of size L. The corresponding velocity scales are u_d and V for the length scales d and L, respectively. Hence, the wall shear stress scales as

$$\tau = -\rho\overline{u'w'} \sim \rho u_d V. \tag{1}$$

Equation 1 is valid for any region of the flow domain in proximity of the wall: the roughness sublayer in uniform flow [26], the scour hole of a bridge pier [24], or, as presented here, the scour region downstream of an MHK turbine. The difference between these cases is the size of the energy containing eddies, i.e. the largest statistically persistent eddy scale. Here we adopt the argument of [24] that the largest eddies within the scour region have characteristic size comparable to the scour depth y_s. For now the characteristic velocity V remains undefined.

As in [24, 26], Kolmogorov's scaling is applied to relate characteristic scales within the inertial range according to the turbulent energy cascade [28]. We assume the turbulent kinetic energy (TKE) production is in equilibrium with the local dissipation rate and that the energy decay scaling relationships remain valid in the flow region where the MHK turbine scour is localized. In other words, we assume the phenomenology of the energy cascade is conserved, with the small scales of turbulence (proportional to the sediment grain size) adjusting themselves in order to dissipate energy in the way and intensity defined by the energy-containing eddies governing the scour mechanisms. Under these assumptions, the TKE decay rate ϵ scales with the characteristic velocities u_d and V as $\epsilon \sim V^3/y_s \sim u_d^3/d$, leading to

$$u_d \sim V \left(\frac{d}{y_s}\right)^{1/3}. \tag{2}$$

Substituting equation 2 into equation 1 leads to

$$\tau \sim \rho V^2 \left(\frac{d}{y_s}\right)^{1/3}. \tag{3}$$

Following [24], we consider the TKE decay rate ϵ as the power per unit mass (P/M) dissipated in the scour region due to the drag force F_d. For an MHK turbine there are two distinct sources of drag which inform two theoretical model cases:

- Model case 1: the bottom tip of the turbine rotor is close enough to the sediment surface that the local scour is promoted directly by the tip vortices or by any other flow structures of the turbine wake.
- Model case 2: drag is induced by accelerated flow between the sediment surface and the turbine rotor bottom tip impinging on the support tower which behaves as a bridge pier.

The two model cases are developed exclusively; case 1 considers drag only from the turbine rotor and case 2 considers drag only from the support tower. A schematic of the two model cases is shown in Figure 1. The framework under clear water conditions is detailed in sections II A and II B. The extension to live bed conditions is presented in section II C.

A. Model case 1: Rotor drag force

As the rotor approaches the bed surface, the vortical structures shed from the turbine components – the root, blade, and tip vortices – are inferred to augment the shear stress

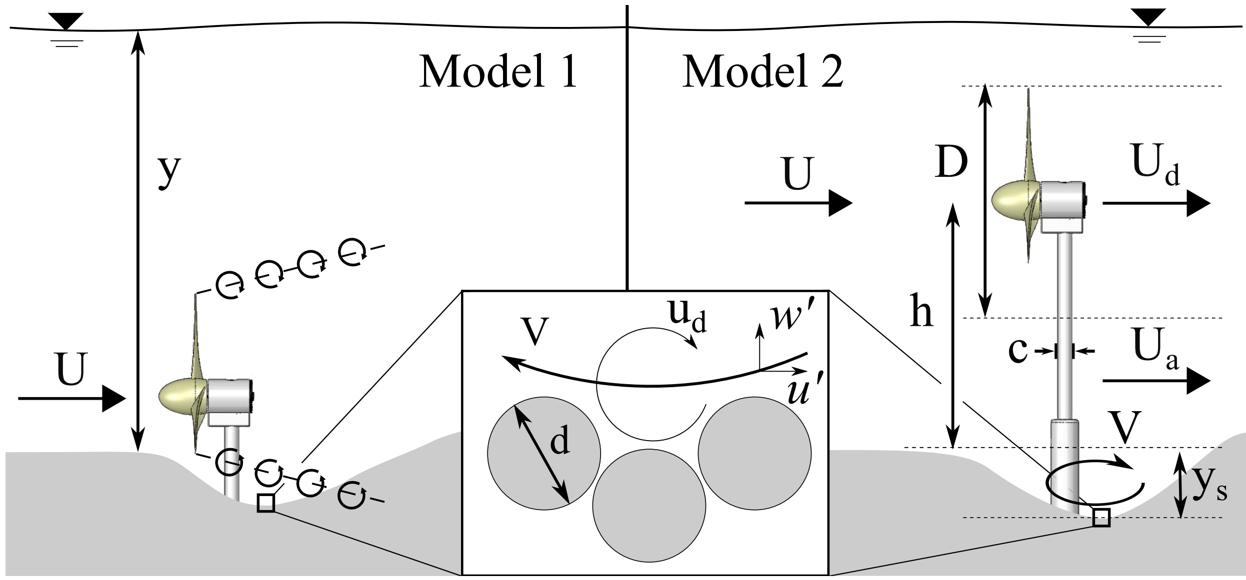

FIG. 1. Schematic of the two theoretical scenarios. Model case 1 (left) considers the effect of the turbine rotor drag on the scour. Model case 2 (right) considers the effect of the support tower drag under accelerated flow. The inset shows the characteristic velocity scales within the scour region.

at the wall and contribute to sediment mobility and scouring. The tip vortices of a turbine are generated by circulation produced along the turbine blades. The circulation is directly related to the power extracted by the turbine, which in turn is related to the drag force exerted by the rotor (see e.g. [29] for utility-scale wind turbines). In model case 1, the intensity of the tip vortices impinging on the bed surface are responsible for the near turbine scour and can be represented using the turbine drag force (or turbine thrust) by incorporating in the formulation the operating conditions and performance of the turbine. As only a portion of the drag exerted by the turbine contributes to the turbulence in the scour region, a correction factor embedded in the model constant will be required. When the rotor vertical position is too high for the tip vortices to interact with the bed surface, the scour mechanism is governed by the horseshoe vortex forming around the support tower, consistent with a bridge pier case [30–33], and model case 1 is not applicable.

To relate the drag force to the turbine operating regime, the turbine is approximated as an actuator disk with an induction factor $a = 1 - U_d/U$, where U_d is the velocity within the porous disk. U is the undisturbed mean velocity measured at the turbine hub height and is assumed to be homogeneous across the rotor plane. The drag force, expressed as the thrust force applied on the actuator disk, is $F_d = \frac{1}{2}\rho C_T A_f U^2$, where the thrust coefficient

$C_T = 4a(1-a)$ depends on the turbine operating conditions and the frontal area depends only on the rotor diameter $A_f = \frac{\pi}{4}D^2$ [34]. Note that the turbine operating condition is defined through the power coefficient dependency on the induction factor, $C_p = 4a(1-a)^2$. The induction factor increases as the tip speed ratio increases from 0, a static rotor, to the optimal tip speed ratio corresponding to the Betz limit ($C_p = 0.593$ and $a = 0.33$). Increasing the power production and induction factor results in a likewise increase in the thrust and drag. However, the drag force and the induction factor are not related in a simple way to power efficiency since hydrodynamic drag, flow separation, and velocity deficit occur in the wake of any structure [35, 36].

Applying a bulk definition of TKE dissipation rate per unit mass in the scour region $\epsilon = P/M$ and assuming that the energy-containing eddies in the rotor wake are predominantly responsible for such a decay, we can rewrite the dissipated power P in terms of the drag force and free stream velocity, leading to

$$\epsilon = \frac{P}{M} \sim \frac{F_d U}{\rho y_s^3}, \tag{4}$$

where the mass M scales as the mass of water within the scour region having linear size y_s (see Fig. 1). Combining equation 4 with $\epsilon \sim V^3/y_s$ and the drag (or thrust) force expression yields

$$\epsilon \sim \frac{D^2 U^3 C_T}{y_s^3} \sim \frac{V^3}{y_s}. \tag{5}$$

The characteristic velocity V of the eddies in the scour region can now be expressed by the following scaling relationship:

$$V \sim U C_T^{1/3} \left(\frac{D}{y_s}\right)^{2/3}. \tag{6}$$

Equation 6 relates the energetic eddies responsible for the turbine scour to both the flow conditions and the turbine parameters. The new definition for V can be substituted into the wall shear stress definition from equation 3:

$$\tau \sim \rho V^2 \left(\frac{d}{y_s}\right)^{1/3} \sim \rho U^2 C_T^{2/3} \left(\frac{D^4 d}{y_s^5}\right)^{1/3}. \tag{7}$$

In the so-called clear water conditions under uniform flow, the wall shear stress τ approaches, but does not exceed, the critical shear stress value τ_c corresponding to the onset of sediment mobility and transport [37]. Thus, bedload transport is negligible except in the proximity of the turbine where the shear stress is locally enhanced. In the wake of the MHK turbine, as well as a bridge pier, erosion occurs until the scour reaches a depth at which the energetic eddies in the scour region can no longer locally exert $\tau > \tau_c$. At that point, an equilibrium condition is reached for a specific sediment size. The equilibrium is expressed as $\tau = \tau_c$ with $\tau_c \sim (\rho_s - \rho)gd$ dimensionally based on Shields' work [37]. Since we are interested in the equilibrium condition corresponding to the maximum scour depth, the shear stress in equation 7 can be considered as the critical stress:

$$\tau \sim \rho U^2 C_T^{2/3} \left(\frac{D^4 d}{y_s^5}\right)^{1/3} \sim \tau_c \sim (\rho_s - \rho)\, gd. \tag{8}$$

Rearranging terms in equation 8 results in an expression for the scour depth y_s:

$$y_s \sim \left(d^{2/3} \frac{\rho_s - \rho}{\rho} \frac{g}{C_T^{2/3} D^{4/3} U^2}\right)^{-3/5}. \tag{9}$$

Introducing the flow depth y to normalize the scour depth y_s yields a relationship between dimensionless groups that are physically relevant to the problem considered here:

$$\frac{y_s}{y} \sim \left(\frac{\rho_s - \rho}{\rho}\right)^{-3/5} \left(\frac{U}{\sqrt{gy}}\right)^{6/5} C_T^{2/5} \left(\frac{D}{d}\right)^{2/5} \left(\frac{D}{y}\right)^{2/5}. \tag{10}$$

The first dimensionless group is the submerged sediment density normalized by the fluid density and can be expressed as $s - 1 = (\rho_s - \rho)/\rho$. The second dimensionless group is the Froude number $Fr = U/\sqrt{gy}$, which represents the ratio between inertial and gravitational forces. Because we employ proportional dependencies in the definition of the shear stress (Eq. 1), the portion of rotor drag responsible for the scour, and the estimate of the Shields critical stress, a multiplicative correction factor K_1 must be introduced to the scaling relationship (Eq. 10), leading to the final equation for the rotor drag force model in clear water conditions:

$$\left(\frac{y_s}{y}\right)_1 = K_1 (s-1)^{-3/5} Fr^{6/5} C_T^{2/5} \left(\frac{D}{d}\right)^{2/5} \left(\frac{D}{y}\right)^{2/5}, \tag{11}$$

where the subscript 1 indicates the rotor drag force model (case 1). The model relationships are as expected: scour will increase for increasing thrust coefficient, rotor diameter, and approaching Froude number (i.e. increasing drag force); scour will decrease for increasing sediment density and size (i.e. increasing critical shear stress).

B. Model case 2: Support tower drag force under accelerated flow

The tower drag force model aligns closely with the bridge pier model of [24]. The turbine bottom tip is considered to be relatively far from the sediment bed such that the tip vortices do not impinge on the wall in the proximity of the turbine. Thus, the rotor drag would not contribute to the scour as directly as the support tower. However, the presence of the rotor induces a flow acceleration in the region between the bottom tip and the sediment bed [27, 38]. To approximate the accelerated flow U_a below the rotor tip (see Fig. 1), mass conservation is imposed in the control volume defined as the flow region extending from the sediment bed to the turbine hub height:

$$U\left(y_t + \frac{D}{2}\right) = U_a y_t + U_d \frac{D}{2}, \tag{12}$$

where y_t is the height from the sediment bed to the turbine bottom tip and U_d is the estimated flow through the turbine rotor as in section II A. Selecting the hub height as the upper bound of the continuity region assumes the flow acceleration is equally distributed around the rotor (i.e. axial-symmetric). Equation 12 also neglects any inhomogeneity in the vertical profile. The validity of these assumptions is assessed in section IV C through the analysis of the turbine hub height h dependency in the model. We define the extent of the acceleration zone y_t as $y_t = h - D/2 = k_t D$ where $k_t = h/D - \frac{1}{2}$. y_t and k_t represent a measure of how close the nacelle is to the wall for a given rotor diameter. Rigorously, y_t should be a function of the scour depth y_s. However, this inclusion leads to a cubic polynomial expression for y_s, of modest practical use. We can neglect the effect of y_s on y_t under two further assumptions: (i) given $y_s << y_t$, we slightly overestimate the velocity U_a impinging on the pier, leading to a conservative estimate of the turbine scour; (ii) more importantly, the scour region is expected to be dominated by a recirculation region scaling with V and y_s, which is fairly decoupled from the incoming flow U_a. Assumption (ii) is consistent with [24], where the incoming velocity onto the exposed pier did not account for the scour depth explicitly, as it was assumed equal to the mean undisturbed velocity in the channel cross section.

Expressing equation 12 in terms of U_a and using the definitions $y_t = k_t D$ and $U_d = (1-a)U$ leads to the following:

$$U_a = U\left(1 + \frac{a}{2k_t}\right). \tag{13}$$

The accelerated flow velocity U_a exerts an enhanced drag on the turbine support tower, which is expected to behave as a bridge pier. From here we can follow [24] literally, applying the drag force equation in the same manner as section II A. Here the tower drag force is $F_d = \frac{1}{2}\rho C_d c y_s U_a^2$, where C_d is the drag coefficient of the tower, c is the tower diameter, and $c y_s$ is the projected area of the tower exposed by scour. Following the procedure of [24] we arrive at the same scour relationship as in the cited text, differing only in the incoming velocity term:

$$y_s \sim \frac{\left(U\left(1+\frac{a}{2k_t}\right)\right)^2}{g}\left(\frac{\rho}{\rho_s-\rho}\right)C_d^{2/3}\left(\frac{c}{d}\right)^{2/3}. \tag{14}$$

As before, we normalize the scour depth by the flow depth y, allowing for use of the Froude number $Fr = U/\sqrt{gy}$. The density is expressed in terms of the submerged sediment specific density $(s-1)$ and a model correction factor K_2 is included, leading to the final equation for the tower drag force model:

$$\left(\frac{y_s}{y}\right)_2 = K_2\,(s-1)^{-1}\,Fr^2 C_d^{2/3}\left(\frac{c}{d}\right)^{2/3}\left(1+\frac{a}{2k_t}\right)^2, \tag{15}$$

where the subscript 2 indicates the tower drag force model (case 2). The scour depth dependencies on the drag force and critical shear stress share some features of the rotor drag model: case 2 predicted scour will increase for increasing support tower drag coefficient, tower diameter, approaching Froude number and decreasing hub height; scour will decrease for increasing sediment density and size (i.e. increasing critical shear stress).

C. Live bed case

In live bed conditions, where $\tau > \tau_c$ away from the turbine in the undisturbed uniform flow, the scour differs from the clear water case due to bedload transport and the formation of bedforms. [24] proposed that the relationship between the live bed scour and the corresponding clear water scour is a power law function of the mean flow intensity. The flow intensity quantifies the excess shear stress above the critical value, and is expressed as U/U_c, where U_c is the critical hub velocity associated with τ_c. Our model can be extended to the live bed condition by adopting the same functional dependency on the incoming to critical velocity ratio proposed by [24], assuming that the live bed regime has the same effects on the scour depth under different drag mechanisms (see section IV B). We use the same scour depth notation S_e [24] for consistency. From equation 11, the rotor drag force model can be formulated as:

$$S_{e1} = \left(\frac{y_s}{y}\right)_1 \left[(s-1)^{-3/5} Fr^{6/5} C_T^{2/5} \left(\frac{D}{d}\right)^{2/5} \left(\frac{D}{y}\right)^{2/5}\right]^{-1} = K_1 \left(\frac{U}{U_c}\right)^{\theta_1}. \tag{16}$$

Similarly, from equation 15, the tower drag force model for live bed conditions is

$$S_{e2} = \left(\frac{y_s}{y}\right)_2 \left[(s-1)^{-1} Fr^2 C_d^{2/3} \left(\frac{c}{d}\right)^{2/3} \left(1 + \frac{a}{2k_t}\right)^2\right]^{-1} = K_2 \left(\frac{U}{U_c}\right)^{\theta_2}. \tag{17}$$

The model coefficients $K_{1,2}$ must be estimated empirically. The power law exponents $\theta_{1,2}$ require special attention as they describe the scour depth dependency with the incoming velocity, which is also implicitly accounted for in the Froude number (addressed in section IV B). Note that the clear water model equations are a subset of the live bed equations above in the particular case that $U = U_c$. The use of a single general equation for clear water and live bed conditions (i.e. a single coefficient K) in each model case permits the combination of experimental results in the different hydraulic and transport regimes, provided the critical velocity U_c and θ are known or estimated empirically. Whereas in the clear water case y_s is the maximum scour depth defining the equilibrium condition, in live bed cases y_s is the average scour depth resulting from temporal averaging of bed elevations over many passing bedforms. Such a distinction is relevant for the estimate of the maximum instantaneous scour depth under live bed conditions (see section IV D).

III. EXPERIMENTAL DATA SET

A. Previous Experiments

A number of experiments have been performed in the past few years and are collected here to validate the proposed theoretical framework. The purpose of these experiments was to study different siting configurations of in-stream MHK turbine(s) in open channel flows over erodible sediment bed, with a primary interest on the effect of migrating bedform types. The experiments, summarized in Table I, were performed at St. Anthony Falls Laboratory (SAFL) at the University of Minnesota. The experiments performed in straight channels (the Titling Bed Flume and the Main Channel) under critical mobility and live bed conditions ([5, 6, 39]) will be used primarily for validation. We will use some caution

Exp.	D [m]	d [m]	h [m]	U [ms^{-1}]	U_c [ms^{-1}]	y [m]	y_s [m]	Transport	Facility
1	0.15	0.0018	0.13	0.46	0.46	0.28	0.024	clear water	TBF
2	0.15	0.00042	0.13	0.33	0.21	0.26	0.021	ripples	TBF
3	0.15	0.0018	0.12	0.6	0.46	0.26	0.035	dunes	TBF
4	0.5	0.0018	0.425	0.66	0.66	1.15	0.15	clear water[1]	MC
5	0.5	0.00042	0.425	0.51	0.31	1.17	0.049	ripples	MC
6	0.5	0.00042	0.425	0.74	0.31	1.17	0.07	dunes	MC
7	0.15	0.0007	0.13	0.67	0.26	0.31	0.022	dunes[2]	OSL
8a	0.15	0.0018	0.092	0.41	0.41	0.26	0.033	clear water	TBF
8b	0.15	0.0018	0.110	0.41	0.41	0.26	0.026	clear water	TBF
8c	0.15	0.0018	0.130	0.41	0.41	0.26	0.019	clear water	TBF
9a	0.15	0.0018	0.107	0.78	0.46	0.26	0.027	dunes[3]	TBF
9b	0.15	0.0018	0.124	0.78	0.46	0.26	0.024	dunes[3]	TBF
9c	0.15	0.0018	0.135	0.78	0.46	0.26	0.019	dunes[3]	TBF

TABLE I. Experimental values including turbine properties (rotor diameter D, hub height h), flow characteristics (free stream hub velocity U, undisturbed flow depth y), sediment transport conditions (mean grain diameter d, critical velocity for incipient motion U_c) and the flow facility (TBF: Tilting Bed Flume, MC: Main Channel, OSL: Outdoor Stream Lab). [1] Indicates the only experiment with a conical base below the turbine support tower; [2] Indicates a non-uniform flow channel with meander; [3] Indicates an asymmetric deployment of two turbines in the same cross section. Additional information on experimental apparatus and measurement techniques can be found in [5] for Exp. 1, 3, 4, in [39] for Exp. 2, 5, 6, in [7] for Exp. 7, and in [40] for Exp. 9 a,b,c. Experiments 8 a,b,c were conducted specifically for this work.

with other experiments performed in more complex conditions, e.g. near the outer bank of a meandering stream (the Outdoor Stream Lab [7]) or in a multi-turbine asymmetric setting designed to favor meandering onset [40]. Indeed, with complex siting or bathymetries, the definition of the critical velocity is not trivial: non-negligible spanwise slope is known to affect critical mobility [41]. Furthermore, the presence of secondary currents alter the shear stress distribution at the wall and thus may affect the dissipative mechanisms downstream of the turbine.

In all experiments, the scour evolution behind the turbine was measured in time and space by continuously scanning the bed elevation using a submersible sonar transducer Olympus Panametrics C305-SU (Olympus NDT, Walthman, MA) with a resolution of ± 1 mm mounted on a data acquisition cart (designed and built at SAFL). The cart is able to automatically travel across the entire surface of the experimental channel. The measurements were collected along a longitudinal transect centered on the turbine y-position. Inflow conditions (U) were monitored using a Nortek Vectrino acoustic doppler velocimiter (ADV) positioned at hub height upstream of the turbine location. The experiments in clear water condition were performed until the local scour reached its equilibrium depth, while live bed condition cases were run and monitored for several hours after the streamwise bed slope reached morphodynamic equilibrium and the bedform-averaged scour depth statistically converged. Additional information about experimental set up and measurement techniques can be found in [5, 6, 39, 40].

Two scales of a three-bladed axial flow turbine were used in these experiments: a small scale model with a rotor diameter $D = 0.15$ m and a large scale model with a rotor diameter $D = 0.5$ m, corresponding respectively to 1:33 and 1:10 scaled versions of a real axial flow turbine design. The small scale model was composed by a resin prototyped rotor (hub and blades) mounted directly on the shaft of a DC motor. The motor allowed for instantaneous voltage measurements and introduced a non-negligible internal frictional torque, thus achieving reasonable tip speed ratio without applying electrical loading on the motor. The nacelle was held on a cylindrical support tower of diameter $c = 0.01$ m. The large scale turbine model design was similar in geometry, with a resin nacelle mounted on a cylindrical tower of diameter $c = 0.04$ m. At this scale the nacelle was equipped with a stepper motor, a torque transducer, and an optical rotary encoder able to precisely control and measure the angular velocity ω and the produced torque in order to match the optimal tip speed ratio λ. Further details on turbine geometry and design information are available in [4].

In addition to the values given in Table I, the sediment specific gravity $s = 2.65$ was the same for all experiments. For the tower drag force model, the cylinder drag coefficient for the support tower is assumed $C_d = 1$, which is representative for the range of Reynolds numbers investigated: $Re = Uc/\nu = 3.3 \times 10^3 - 6.6 \times 10^4$, where c is the cylinder diameter and the hub velocity U is the incoming velocity.

B. New Experiments

A new set of experiments (8 a,b,c in Table I) were performed, specifically to address the dependency of model case 2 on the hub elevation and to investigate a potential transition between case 2 and case 1 as the bottom tip approaches the bed surface and the rotor drag is inferred to start governing the scour depth. Three configurations under the same hydraulic conditions were tested, varying only the hub height h above the bed. The hydraulic conditions were the same as in [5] for the single turbine clear water case (experiment 1 in table I).

The thrust coefficients of the turbine models were estimated in two different ways. The large scale MHK turbine model ($D = 0.5$ m), used in the Main Channel facility, was operated at optimal tip speed ratio and blade pitch angle with a peak power coefficient $C_p \simeq 0.40$ [39]. Hence, we employ an induction factor $a = 0.33$ corresponding to peak production as in the actuator disk model [34] to calculate the thrust coefficient $C_T = 4a(1-a) = 0.88$. For the small turbine model ($D = 0.15$ m), the actuator disk assumptions do not hold because the imposed torque was frictional and not optimal. As no supporting theory was available for the estimate of the thrust coefficient, direct drag force measurements were performed by towing the rotor (mounted upside-down) at different speeds through the main channel in still water conditions (not shown here). Thrust coefficients for the small scale turbine experiments were estimated using an empirical $C_T - Re$ relationship derived from direct drag measurements. The thrust coefficient range for these experiments $C_T \approx 0.7$ to 0.9 for $Re = UD/\nu = 5 - 11 \times 10^4$, is comparable to the coefficient for the large scale turbine model despite having a lower power coefficient. This result highlights the fact that thrust and power are only correlated for a high performing turbine for which the actuator disk model works, and that a relatively low performing turbine can generate a significant drag (see, e.g. [36] comparing wakes of a 2.5MW wind turbine in the atmospheric surface layer and a miniature model in a wind tunnel). Because the drag force is unambiguously related to the mean velocity deficit, we estimated the actuation factor a for the small scale turbine case from the measured thrust coefficient using $C_T = 4a(1-a)$, stressing again that the corresponding relationship with the power coefficient cannot be employed.

IV. VALIDATION

A. Model Proportionality Constants

For both cases derived in section II, functional dependencies were introduced with proportionality constants that are not explicitly defined, but collectively contribute to the two case-specific constants K_1 and K_2. We expect the two drag force mechanisms (accounted for separately in the two cases) may both contribute to scour production at varying degrees in a given turbine configuration. For this reason, and due to the relatively small number of experimental points, we define K_1 and K_2 coefficients using a value range rather than attempting to fit a single value.

In Figures 2a and 2b we plot the scour depth function S_e versus the flow intensity U/U_c using model equations 16 and 17, respectively. The data markers in the figure legend correspond to the experiments tabulated in Table I. The experimental points in Fig. 2 contain both the measured scour and the functional dependencies of the model, i.e. the left sides of equations 16 and 17; the model curves (dashed lines) represent the right sides of the same equations using $\theta_1 = -1.89$ and $\theta_2 = -1.1$, respectively. The selection of θ values is described in section IV B below. The predicted model coefficient ranges, $K_1 = 0.075$ to 0.21 and $K_2 = 0.17$ to 0.40, cover all the experimental results.

B. Model Power Coefficients

Determination of the power law coefficients θ_1 and θ_2 is particularly difficult. The scatter of the experimental points and the limited flow intensity range $U/U_c = 1 - 2.5$ shown in Fig. 2 preclude a precise power law fit with a narrow confidence range. Instead of prescribing a fit, we discuss the coefficients in view of previous results and comparative theoretical arguments.

In the pure bridge scour case, θ was estimated by [24] as $\theta = -1.89$ using a very large set of data from the literature, suggesting that when the critical mobility stress is exceeded, the scour remains only marginally dependent on the flow velocity: $y_s \propto U^{0.11}$ resulting from $y_s \propto U^2$ in the clear water case and $U^{-1.89}$ in the live bed correction. This weak dependency is consistent with the results reported in the pioneering work of [42]. The interpretation of this weak dependency is two-fold: i) the live bed excess shear stress mobilizes sediments that

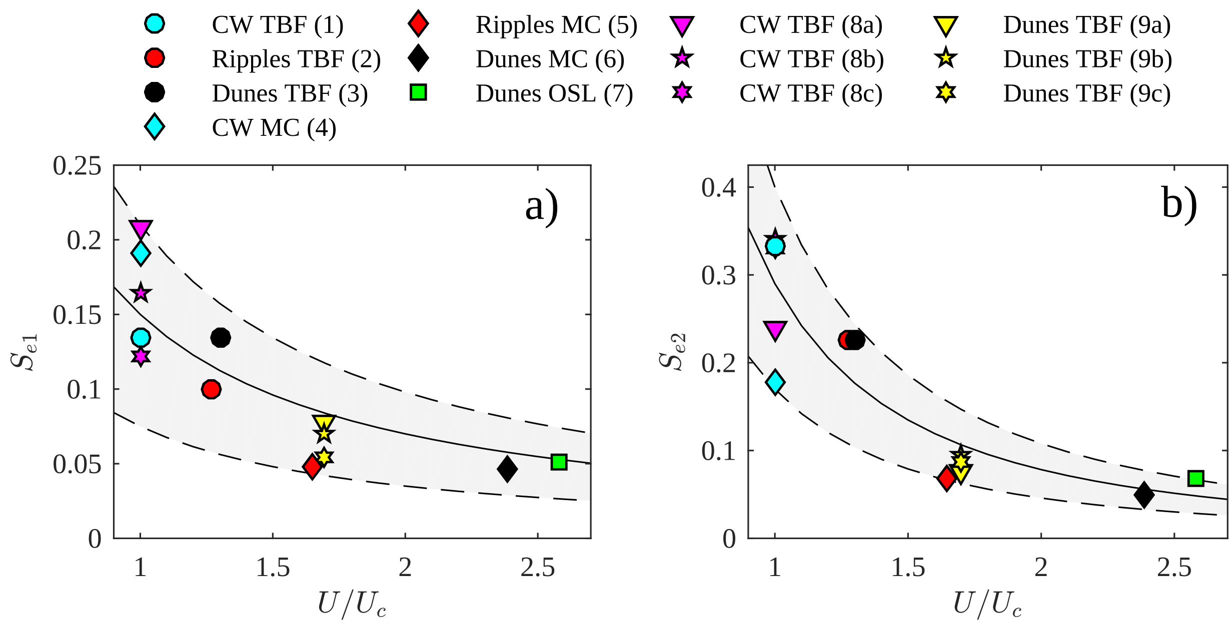

FIG. 2. Experimental values of the scour depth function S_e compared to the model curves for a) the rotor drag, model case 1 (Eq. 16), with dashed lines indicating coefficient range $K_1 = 0.075$ to 0.21 and the solid line indicating the midpoint $K_1 = 0.15$; b) tower drag, model case 2 (Eq. 17), with dashed lines indicating coefficient range $K_2 = 0.17$ to 0.40 and the solid line indicating the midpoint $K_2 = 0.29$. The model curves follow the form $S_e = K(U/U_c)^{\theta}$ where $\theta_1 = -1.1$ and $\theta_2 = -1.89$. $U/U_c = 1$ indicates clear water (CW) conditions.

are transported as a bedload sheet with a thickness proportional to the shear penetration in the granular substrate and with the deepest mobilized layer in critical conditions, consistent with the hypothesis of Bagnold [43]; ii) larger shear stress and sediment flux generates larger bedforms which absorb more streamwise momentum and induce more drag, thus limiting the increase of local scour. Because the response of erodible sediments to migrating bedforms and bedload transport should be somewhat independent from the nature of the forcing (the shear stress applied to the bed surface), we expect that MHK turbines local scour in live bed will manifest the same weak positive dependence on the incoming flow velocity that has been demonstrated to govern bridge pier scour. Because model case 2 presents the same Froude dependency of [24], the same coefficient $\theta_2 = -1.89$ was adopted. In turn, for model case 1 we use $\theta_1 = -1.1$ to maintain the same live bed dependency $y_s \propto U^{0.11}$. Note that θ changed for model case 1 because the Froude power coefficient and thus the hub velocity dependency is different beyween case 1 and case 2.

C. Functional Dependencies

To verify the theoretical model, the functional dependencies derived in the model equations must be validated (see Figures 3 and 4). The Froude dependency for both cases is first investigated (Figures 3a for case 1 and 4a for case 2), albeit not in a fully independent manner. The hub velocity and incoming flow depth terms contributing to the Froude number appear also in other dimensionless terms of the model equations, such that varying the Froude number changes other parameters as well. The Froude dependency is particularly important because it highlights one of the few key differences between the two model cases: $(y_s/y)_1 \sim Fr^{6/5}$ versus $(y_s/y)_2 \sim Fr^2$. The difference provides a possible objective path to rank the representativeness of the two cases. To compare dependencies, we rearranged the terms of equations 16 and 17, leaving the Froude number on the right hand side and the remaining dimensionless quantities on the left hand side:

$$\left(\frac{y_s}{y}\right)_1 \left[\left(\frac{U}{U_c}\right)^{\theta} (s-1)^{-3/5} C_T^{2/5} \left(\frac{D}{d}\right)^{2/5} \left(\frac{D}{y}\right)^{2/5}\right]^{-1} = K_1 Fr^{6/5} \tag{18}$$

for the rotor drag force (model case 1), and

$$\left(\frac{y_s}{y_1}\right)_2 \left[\left(\frac{U}{U_c}\right)^{\theta} (s-1)^{-1} C_d^{2/3} \left(\frac{c}{d}\right)^{2/3} \left(1+\frac{a}{2k_t}\right)^2\right]^{-1} = K_2 Fr^2 \tag{19}$$

for the tower drag force (model case 2). The left hand side of equations 18 and 19 can be interpreted as (y_s/y) normalized by the terms within the square brackets and expressed as $\widetilde{(y_s/y)}$. The graphical representation of the experimental measurements in the $\widetilde{(y_s/y)}, Fr$ phase space is depicted in Figures 3a and 4a.

The range of experimental facilities and turbine models investigated has enabled us to also test the y_s/y dependency on D/d for model case 1 (Fig. 3b), and on the submergence parameter $1+a/2k_t$ for model case 2 (Fig. 4b). The former shows the clear water experiments with the small MHK turbine model (Tilting Bed Flume, experiment 1) and large model (Main Channel, experiment 4). By comparing only clear water results we avoid potential contamination from uncertainty in θ or the critical velocity U_c. A power law (solid line) representing a best fit of the data is included for visualization of the dependency agreement. Although we acknowledge that two points represent a weak demonstration, the agreement is surprisingly good even with evident uncertainty on the model coefficient K_1 (dashed lines). Fig. 4b demonstrates the $1+a/2k_t$ parameter dependency of model case 2 using clear water

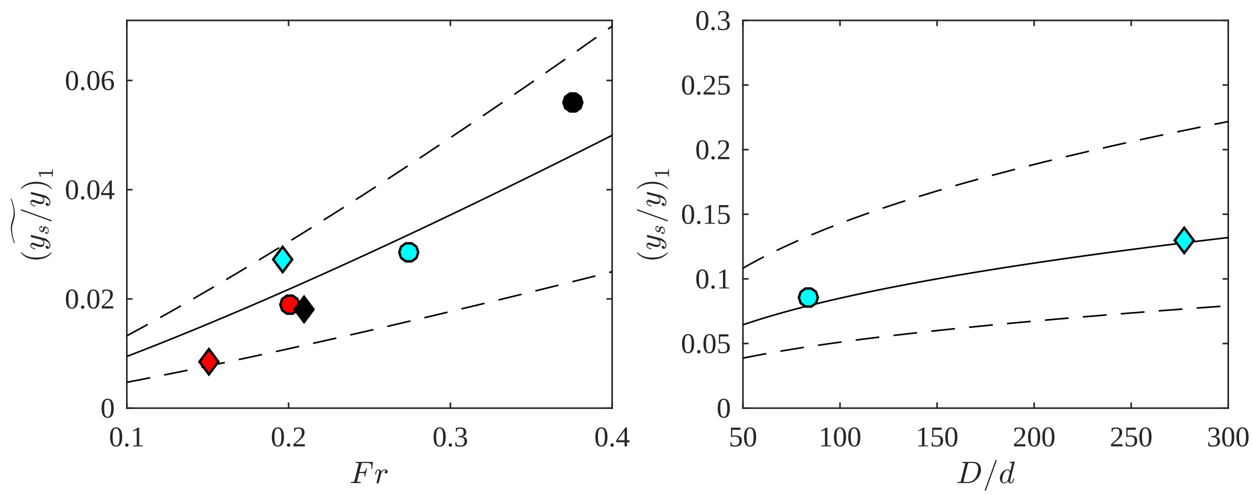

FIG. 3. Functional dependency of the rotor drag (model case 1) on the a) Froude number Fr where $(\widetilde{y_s/y})_1 = \left(\frac{y_s}{y}\right)_1 \left[\left(\frac{U}{U_c}\right)^{\theta} (s-1)^{-3/5} C_T^{2/5} \left(\frac{D}{d}\right)^{2/5} \left(\frac{D}{y}\right)^{2/5}\right]^{-1}$ is the left hand side in equation 18, and b) rotor diameter normalized by the sediment size D/d. The solid lines represent the best fit of the experimental data for the theoretically derived power laws: a) $Fr^{6/5}$ b) $(D/d)^{2/5}$. The dashed lines mark the bounds of the coefficient range $K_1 = 0.075$-0.21. Refer to Fig. 2 for data marker definitions.

experiment 8 and live bed experiment 9. In both experiments the scour depth was measured for three different turbine hub heights under otherwise identical conditions. Coincidentally, a single power law fits both sets of data; the fit line uses $K_2 = 0.27$ for experiment 8 and $K_2 = 0.24$ for experiment 9, both within the coefficient range $K_2 = 0.17$ to 0.40. For the lowest turbine height (8a), there is a clear departure from the proposed $1+a/2k_t$ dependency. As the distance from the bed to the bottom tip decreases, we expect a transition from the tower drag force model case 2 to the rotor drag force model case 1 as the dominant scour mechanism (dashed lines indicate the scour depth predicted by model case 1, for reference). Fig. 4b is consistent with this expectation, and suggests that the tower drag force model case 2 is valid for $1+a/2k_t < 2$, but not for $1+a/2k_t > 2.5$ where model case 1 should apply. Note that the apparent transition range $1 + a/2k_t$=2-2.5 corresponds to $h/D = 0.61 - 0.65$ under optimal conditions (a=0.33).

The functional dependency analysis indicates that the model works well to predict scour across a relatively wide experimental parameter space within the uncertainty indicated by the range of model coefficient K values. The scatter in the Froude dependency suggests

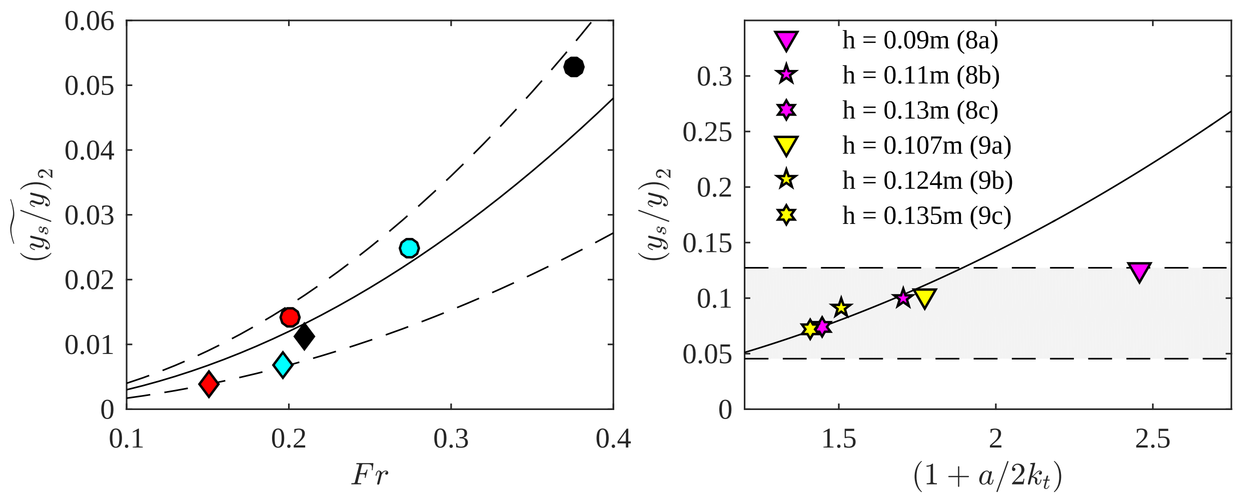

FIG. 4. Functional dependency of the tower drag (model case 2) on the a) Froude number Fr where $\widetilde{(y_s/y)}_2 = \left(\frac{y_s}{y_1}\right)_2 \left[\left(\frac{U}{U_c}\right)^{\theta}(s-1)^{-1} C_d^{2/3} \left(\frac{c}{d}\right)^{2/3} \left(1+\frac{a}{2k_t}\right)^2\right]^{-1}$ is the left hand side in equation 19, and b) rotor submergence represented by $1 + a/2k_t$. The solid lines represent the best fit of the experimental data for the derived power laws: a) Fr^2, b) $(1 + a/2k_t)^2$. In a) the dashed lines indicate the bounds of the coefficient range $K_2 = 0.17$-0.40, while in b) the dashed lines indicate the model case 1 scour prediction range with $K_1 = 0.075$-0.21 for comparison. Refer to Fig. 2 for data marker definitions.

the support tower drag to be the more dominant mechanism in generating scour under the majority of the conditions investigated so far. However, the tower drag force model becomes less dominant as the turbine bottom tip moves closer to the wall. For a class of MHK turbines integrated with a support structure close to the sediment bed (e.g. Openhydro [44]) or designed to maximize rotor diameter while ensuring river navigability in relatively shallow rivers, model case 1 is expected to provide more physically representative scour depth predictions.

The following model dependencies cannot be independently validated with the available experimental data: C_T and D/y for model case 1, C_d and c/d for model case 2, and $(s-1)$ for both cases.

D. Local scour under migrating bedforms: a probabilistic approach for maximum scour depth

As previously stated, for live bed conditions the model prediction of y_s is the average scour and does not consider the variability of scour depth in time due to bedform migration. However, in the context of engineering design, the maximum scour behind the support tower is more relevant than the average to anticipate exposure of the tower foundation and avoid the structural collapse of the MHK turbine. For this reason, we extend here the former analysis with a probabilistic approach for two live bed experiments: ripples in the Main Channel (experiment 5) and dunes in the Tilting Bed Flume (experiment 3). Instead of the mean scour, we consider the entire distribution of scour depths monitored under migrating ripples and dunes.

Figures 5a and 5b show the time-resolved depth measurements as a function of the streamwise distance from the turbine (x_T) for the ripples and dunes experiments, respectively. The vertical axes of the two figures are scaled such that they represent the same physical distance. Figures 5c and 5d show the corresponding probability density functions (PDFs) of the scour depth for the measurement points immediately downstream of the turbine. The PDFs include reference lines for the average scour (solid) and one bedform amplitude greater than the average (dashed), where the bedform amplitude A_{bf} is one half the bedform crest-to-trough height. The small variability in scour depth relative to the bedform amplitude for the ripples case indicates that the localized erosion process prevails over the ripples migration in the scour region. The opposite is true in the dunes case where significant variability is introduced by the larger bedforms. The non-Gaussian distribution of scour depth in the dunes case is skewed right and the maximum scour depth is approximately two bedform amplitudes (thus approximately one bedform height) greater than the mean. The significantly different contributions from the two bedform types to the scour variability is due to the different bedform amplitude relative to the predicted clear water scour depth.

In Fig. 6a, the PDFs of Fig. 5 are related to the model coefficient values K_1 and K_2. The corresponding cumulative density functions (CDFs) are shown in Fig. 6b. The distribution of scour depths are compared to the defined ranges for the model case 1 coefficient (dot-dashed lines, bottom horizontal axis) and the model case 2 coefficient (dashed lines, top horizontal axis). The distribution of scour for the ripples experiment is narrow along the K-

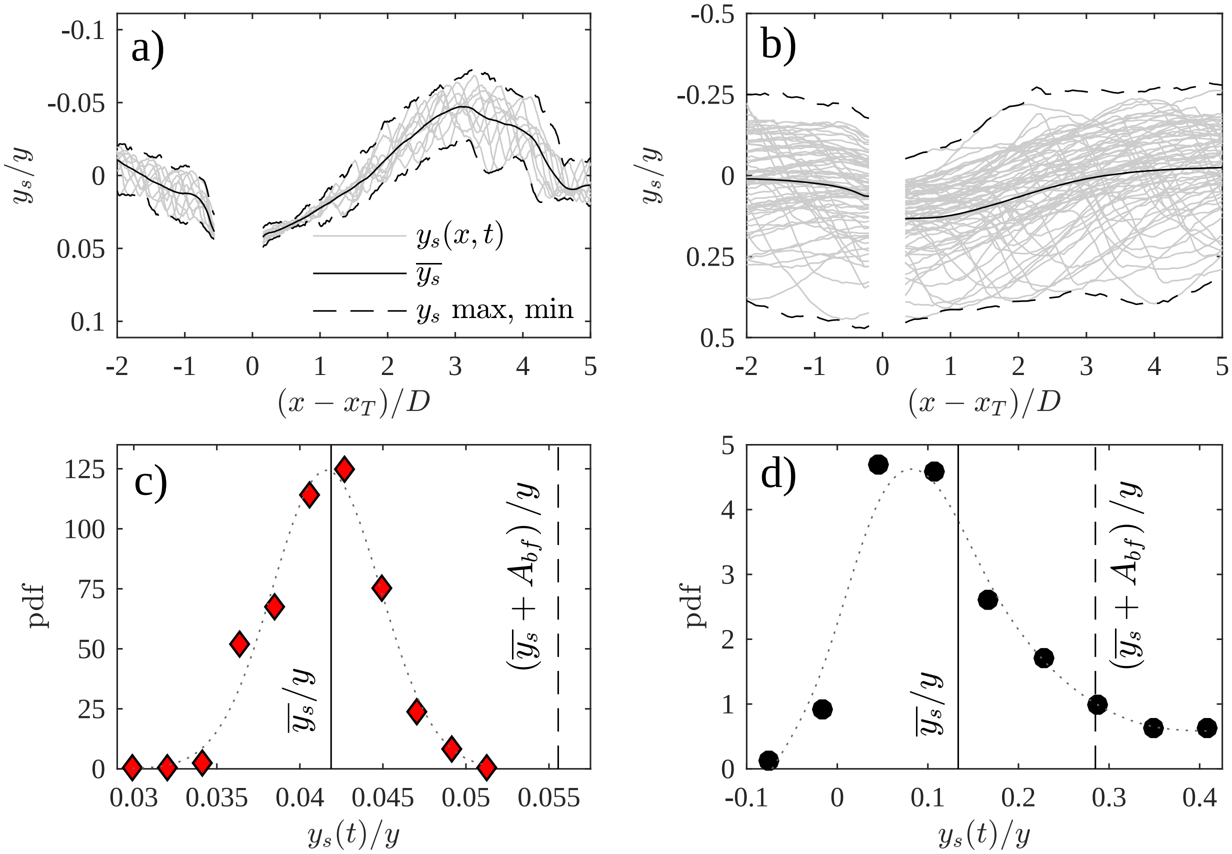

FIG. 5. Time-resolved bed elevation measurements (gray lines) downstream of the MHK turbine, located at $(x - x_T)/D = 0$, for a) experiment 5 (ripples in the Main Channel); b) experiment 3 (dunes in the Tilting Bed Flume). Average scour (solid black line) and minimum and maximum (dashed lines) bed elevation envelops are included for reference. Probability density function of instantaneous scour depth immediately downstream of the turbine for c) experiment 5; d) experiment 3. Average scour depth $\overline{y_s}$ (solid line) and bedform amplitude A_{bf} (dashed line) are indicated.

axis with nearly the entire distribution residing within the coefficient limits (Fig. 6a). The dunes experiment covers a much broader K-axis range, with the coefficient related to the maximum scour is 3-4 times the one related to the averaged scour depth for both cases. For ripples, the difference between average and maximum scour is within the uncertainty range of the model coefficients and requires no secondary assessment. For dunes, the distribution exceeds the model coefficient range and requires additional consideration to relate average and maximum scour.

The maximum scour can be represented as a factor of the predicted average scour (and

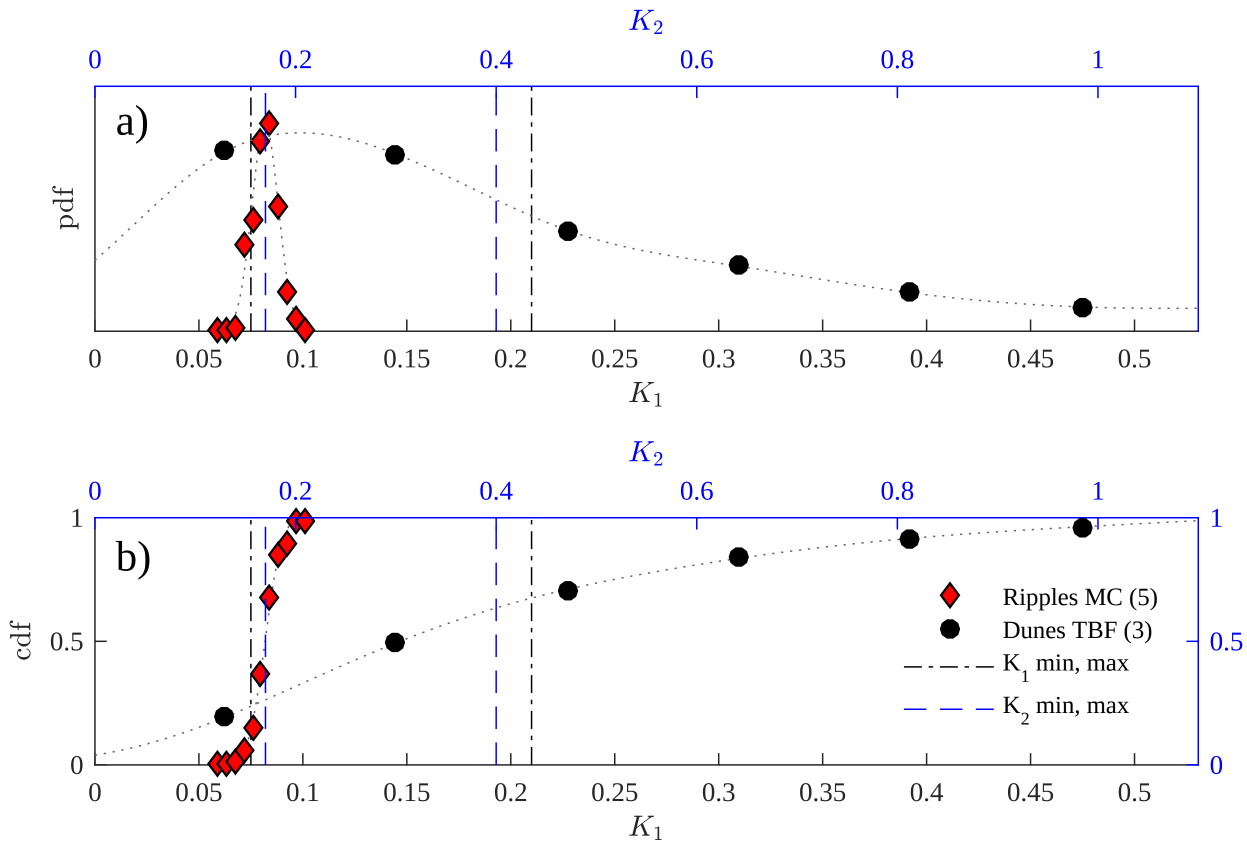

FIG. 6. a) Probability density function of model coefficients K_1 (bottom axis) and K_2 (top axis) corresponding to the instantaneously measured scour depths reported in Fig. 5c,d immediately downstream of the turbine, for experiments 3 and 5. b) Cumulative density function for the same quantities. Prescribed ranges for K_1 and K_2 included are for reference.

perhaps the bedform amplitude) or as a percentile of the scour probability distribution. For the latter, the proportionality constant K would be replaced by a distribution with each constant corresponding to a probability to exceed a certain value. For example, under large dunes the scour predicted by the rotor drag force model $K_1(90\%) = 0.37 \rightarrow y_s/y = 0.28$ would be exceeded 10% of the time, as compared to the mean scour $y_s/y = 0.14$ predicted by $K_1 = 0.18$ which could be exceeded 40% of the time (see Fig. 6b). In either case, a separate model would be required to predict the scour factor or coefficient probability curve under migrating bedforms. Such a model would be highly beneficial given the potentially high discrepancy between a conservative (e.g. employing $K_1(90\%)$) and an average scour prediction.

V. DISCUSSION: HUB VELOCITY AND FIELD-SCALE ESTIMATES

To ensure the applicability of the presented model, we discuss here the choice of the hub velocity scaling quantity and provide a sample of the model predictive capabilities in a utility-scale deployment. On the first issue, the channel mean cross-sectional velocity would be a more accessible velocity scale, from a hydraulic perspective, to be implemented in the model. However, in light of power production estimation and resource assessment, we opt for a site-dependent velocity providing a more local and accurate estimate of the available mean kinetic energy and bed scouring potential. Based on measured vertical profiles of mean velocity in the Tilting Bed Flume and Main Channel facilities, the hub velocity and the channel mean-cross sectional velocity were observed to be quite close [5] (although this has to depend also on the specific turbine geometry). Significant differences and potential scaling implications arise with deployments in more complex bathymetries, e.g. in the Outer Stream Lab experiment, where the spanwise variability of the mean velocity in the meander section is notable (see [7, 45]) and the mean cross-sectional velocity may not be an adequate incoming velocity scale for both turbine operating conditions and local geomorphic effects. However, by choosing instead the local hub velocity, we would face some uncertainty in the critical velocity U_c, defined as the hub velocity at which critical mobility occurs, as opposed to the critical mean cross-sectional velocity typically reported in the literature. For a rigorous application in complex channel geometries or multi-turbine arrays, the support of high fidelity numerical simulations would be advantageous [e.g. 27, 45–49]; alternatively, local measurements with Acoustic Doppler Profiler at the site should be sufficient for both assessing energy resources and estimating the model input velocity for scour prediction [see e.g. 50–52].

As a tangible outcome of this investigation, a turbine scour predictive analysis is provided here for a potential prototype-scale deployment to give a qualitative and quantitative idea of the anchoring system required in large scale sandy rivers. We do acknowledge that the functional dependency of the model have been tested on limited ranges of the parameters involved, nevertheless we believe it is important to provide a quantitative assessment on the feasibility of a MHK utility-scale installation. We base our analysis on the lower Mississippi river using the high quality data provided in [53]. The river section in Audubon Park, New Orleans, Louisiana is a reasonable deployment site given the 25 m large depth, the straight

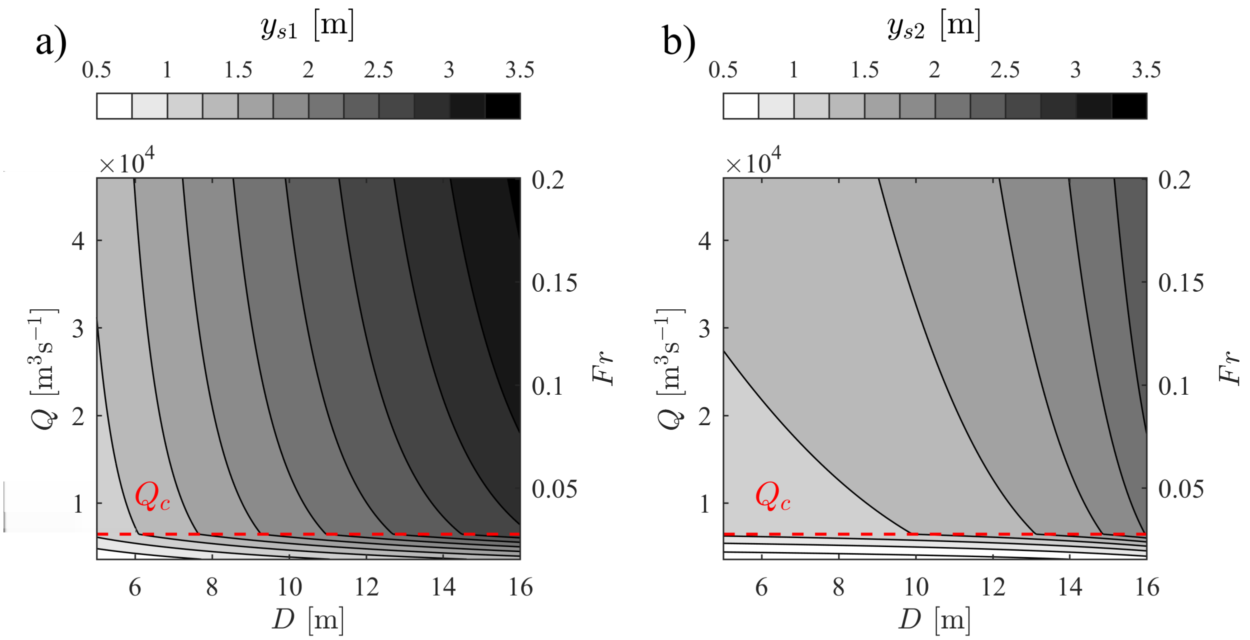

FIG. 7. Predicted scour depth in the Mississippi River at Audubon Park, New Orleans, LA, as a function of the flow discharge and rotor diameter for a) model case 1 using $K_1 = 0.15$ and b) model case 2 using $K_2 = 0.29$. This estimation assumes optimal turbine performance, fixed local depth $y = 25$ m, river width $b = 600$ m, median grain size $d = 0.0002$ m, critical velocity $U_c = 0.42$ ms^{-1}, support tower diameter $c = 1$ m and drag coefficient $C_d = 1$. For model case 2 the turbine top tip elevation is fixed 3 m below the water surface. The red dotted line indicates the discharge Q_c corresponding to the critical flow velocity for the sediment incipient motion and thus to the transition between clear water equations 11,15, and live bed equations 16,17. The critical flow velocity for the median grain size employed was estimated following [20, 21].

channel morphology (width of approximately 600 m), and the high flow discharge. Because of the downstream level control exerted by the ocean, we assume the dominant effect of the flow discharge variation is on the velocity scale U and not on the flow depth. This assumption is consistent with the high variability of the measured mean flow velocity in the cited dataset. Therefore, for the given width we can map the model scour predictions for varying rotor size and flow velocity (Fig. 7). We test a rotor diameter range $D = 5 - 16$ m and a velocity range $U = 0.24 - 3.14$ ms^{-1}. The velocity range is consistent with [53], and is expressed here as a function of both the discharge Q and Froude number Fr. Assuming optimal performance, median grain size $d = 0.2$ mm and critical hub velocity of $U_c = 0.42$ ms^{-1}

(estimated following [20, 21]), model case 1 predicts scour depths of 0.5-3.5 m, corresponding to $y_s/y = 0.02 - 0.14$ (Fig. 7a). For model case 2 we assume the turbine rotor will be located far from the river bed, with an invariant clearance $cl = 3$ m between the top tip and the water surface, and supported by a cylindrical tower of 1 m diameter with a drag coefficient of 1.0. The invariant clearance and rotor diameter range result in k_t variations, which, combined with the discharge variability, lead to model case 2 scour depth predictions of 0.5-2.5 m (Fig. 7b). The scour depths are predicted using middle values of the model coefficient ranges $K_1 = 0.15$, $K_2 = 0.29$. The predicted scour depth in Fig. 7 illustrates the weak dependence on the flow velocity and the importance of the rotor diameter. Note that the application of the two model scenarios is conducted independently. Model case 1 is based on the assumption that the bottom tip is always in the proximity of the channel bed and thus no transition to case 2 would occur. The diameter is in fact increased by raising the upper tip elevation along with the hub height. Conversely, for model case 2 the upper tip elevation is fixed at an invariant clearance $cl = 3$ m, with respect to the free surface; as the diameter increases, the hub height and the gap between the bottom tip and the bed surface (y_t) decrease. Hence, in this scenario we might expect a transition from case 2 to case 1. The experiments performed at different hub height (Fig. 4b) suggest that for $(1 + a/2k_t) > 2.5$, model case 2 is no longer applicable. Recalling that $k_t = y_t/D$ (see Section IV C), we can obtain the dimensional gap limit as $y_{lim} = aD/3$. The equation suggests that the elevation limit increases as the D increases, which is intuitively sound. For this specific scenario where the depth and the clearance between the rotor top tip and the water surface are fixed, the gap between the bottom tip and the channel bed can be expressed as $y_t = y - cl - D$. In the limiting case $y_t = y_{lim}$ the rotor diameter at which model case 2 is no longer applicable is estimated as: $D_{lim} = \frac{3(y-cl)}{a+3} = 19.8$ m, for the specific depth, clearance and turbine performance investigated here. We must however note that the instantaneous bathymetry in rivers with active sediment transport, as in this case study, changes periodically under migrating bedforms. Dunes in the Lower Mississippi can reach heights up to 10 m for extremely high discharges (see measurements by [53] at Audubon Park for a flood event in January 2005). In this case the bed surface would periodically be 5 meters higher, equivalent to the dune amplitude, with respect to the average bed elevation. Taking such conservative local depth value, the rotor diameter limit would reduce to $D_{lim} = 15.3$ m.

To account for the estimated ranges of the constant $K_{1,2}$ and the uncertainties on the estimate of the sediment size, which is inherently related to the critical flow velocity U_c, a reference scenario was chosen to show the potential variability of the estimated scour depth. We opted for a relatively large rotor $D = 10$ m and a medium-high discharge of $Q = 25000$ m^{3}s^{-1}. The corresponding Froude number and the dimensionless parameter k_t for the bottom clearance for model case 2 are respectively $Fr = 0.11$ and $k_t = 1.2$. The other parameters were kept consistent with the case study as listed in the Fig. 7 caption. By varying constants K_1 and K_2 within their estimated ranges, the predicted scour depth is in the interval 1 - 2.9 m for model case 1 and 0.9 - 2 m for model case 2. Finally, to show the variability introduced by the uncertainty on the sediment grain size and thus on the corresponding critical flow velocity for sediment incipient motion, the scour was predicted using the d_{16} and d_{84} percentiles of the particle size distribution, as measured in the survey carried out in 1989 by the US Army Corps of Engineers in the Lower Mississippi [54]. The statistics computed at Audubon Park (the location where we based our upscaling exercise) report $d_{16} = 0.16$ mm and $d_{84} = 0.3$ mm, which correspond to a threshold mean flow velocity U_c of 0.43 ms^{-1} and 0.45 ms^{-1}, respectively. The corresponding estimated scour depths, using the model coefficients middle values $K_1 = 0.15$, $K_2 = 0.29$, were 2.3 m and 1.9 m (model case 1), 1.7 m and 1.2 m (model case 2). Note that the variability in the predicted scour region associated with the occurrence of bedforms is accounted for in the ranges of K_1 and K_2, obtained experimentally, and not explicitly in the critical velocity estimation.

The qualitative trends outlined in the scour depth contours and the related quantitative predictions confirm that prototype deployments in large scale sandy rivers are feasible in the sense that anchoring systems exist to accommodate the mean predictive scour depths, albeit the effect of bedforms on maximum scour has to be included. Note that the issues addressed here are critical for the overall investment due to the significance of anchoring costs (e.g. up to 30% of the total cost for offshore wind turbines [55]). Therefore, the choice of the rotor diameter becomes very important not only for power production but also for erosion protection of the support system.

VI. CONCLUSION

The present work proposes an analytical formulation to predict local scour around Marine Hydrokinetic turbine structures deployed in fluvial or tidal environments characterized by an erodible bed surface. The model builds on the theoretical investigation by [24], which addresses the problem of bridge pier scour using the phenomenological theory of turbulence formulated by [25, 26]. Precisely, the evolution of the scour behind a structure immersed in flowing water, i.e. a bridge pier in [24] or an MHK turbine here, is shown to be governed by geometry-specific turbulent structures that are adjusting themselves in order to dissipate kinetic energy down to the sediment grain scale, at a rate defined by the power dissipated through the drag force exerted by the structure itself. We speculate that the dissipative mechanisms induced by a MHK turbine near the bed surface can be accounted for using two different conceptual cases depending on the relative position of the rotor within the river depth. The turbine rotor may be close enough to the sediments that the erosion is caused directly by the tip vortex shed by the turbine blades or any other turbulent structures in the wake, and consequently related to both the power extracted and the drag force induced by the turbine. Alternatively, the rotor may be far enough that the dominant flow features resemble those responsible for the bridge pier scour, albeit with an augmented incoming velocity due to the flow acceleration between the bottom tip and the bed. To address the different configurations, two model cases were derived and validated covering both clear water (no sediment mobility except for in the proximity of the device) and live bed (under sediment transport and migrating bedforms) conditions, with the extension to the live bed regime through a power law function of the excess shear stress above the critical mobility value.

The experimental validation, performed using spatio-temporal bed elevation measurements with model turbines of different rotor in flumes of different size, allowed us to define a range for the model's coefficients and to confirm the functional dependencies derived theoretically. The authors acknowledge that both the evaluation of the model parameters and the validation of the functional dependencies are affected by uncertainty due to the limited experimental dataset, combined with variability in turbine geometries, river bathymetries, transport conditions and siting configurations. Such an uncertainty in the predicted averaged scour depth is compared to the corresponding variability experienced under migrating bedforms, which cyclically augment and dampen the scour depth. It is indeed important for the structural stability and proper anchoring of the turbine to define under which conditions the turbine base will never be exposed directly to the action of the flow. A probability analysis has shown that the range of scour depth covered by the uncertainty in the model coefficients depends on the inflow migrating bedforms. For large dunes, the maximum instantaneous scour depth can reach values up to two bedforms amplitude (or one bedform height) above the mean scour, exceeding the estimated range of model coefficients $K_{1,2}$ calibrated to the mean scour depth. With migrating ripples, the range of coefficients proposed here was shown to capture the full variability of scour distribution. This means that large dunes, as compared to ripples, may pose a threat to the turbine structural safety if not taken into account. To quantify this risk we propose an approach to select a model coefficient value from a known probabilistic distribution associated to maximum scour probability.

Finally, the validated model was applied to a potential field scale scenario in the lower Mississippi river, where the scour depths have been mapped as a function of the rotor diameter of the prototype turbine, and the actual flow discharge. The predicted scour depths show that deployments of MHK turbines in large scale sandy rivers are feasible.

The developed predictive framework is expected to support the renewable energy engineering community in the expansion of hydrokinetic technology in fluvial environments . Our model provides scour depth estimates required for the siting and design of MHK turbine anchoring systems, relying on simple explicit equations and easily measurable input parameters (the median sediment size and the mean velocity at hub height) obtained through minimal in situ point measurements prior to installation. Besides practical applications, the present study also provides insights into some fundamental mechanics of turbulent flows. All models inspired by [25] provide a correct formulation of the largest and most energetic eddies of the flow and the non-universal mechanism at which turbulent kinetic energy is produced. For instance, this latter can be represented by: the secondary current in an open channel flow [25](recently revised by [56]), the impinging jet on an erodible bed [26], the drag force exerted by a cylinder [24], or, as in the present study, by an MHK turbine rotor. By further assuming a Kolmogorov cascade ensuring equilibrium between production and dissipation, in fact, those models correctly identify the key velocity scale at the intersection between the production and the inertial ranges of the turbulent spectrum. This very same scale is coupled with the near-dissipative scales in the roughness sublayer, in a mixed scaling formulation of the Reynolds stresses [25] that reflects the transfer of energy from the outer scales down to the wall in the physical domain. We speculate that the correct formulation of the turbulent kinetic energy transfer, in both spectral and physical domain, is critical for the extension of this theoretical framework to an even broader range of fundamental and applied problems.

ACKNOWLEDGMENTS

This work was supported by National Science Foundation (NSF) Career Grant Geophysical Flow Control (Michele Guala), NSF PFI grant IIP-1318201, and by CEGE Department fellowships awarded to PhD students M. Musa and M. Heisel.

---

[1] Verdant Power, `http://www.verdantpower.com/`, [Accessed on 2 Novermber 2017].

[2] Ocean Renewable Power Company (ORPC), `http://www.orpc.co/`, [Accessed on 2 Novermber 2017].

[3] Ocean Power Technologies (OPT), `www.oceanpowertechnologies.com/`, [Accessed on 2 Novermber 2017].

[4] LP Chamorro, C Hill, S Morton, C Ellis, REA Arndt, and F Sotiropoulos, "On the interaction between a turbulent open channel flow and an axial-flow turbine," Journal of Fluid Mechanics **716**, 658–670 (2013).

[5] Craig Hill, Mirko Musa, Leonardo P Chamorro, Chris Ellis, and Michele Guala, "Local scour around a model hydrokinetic turbine in an erodible channel," Journal of Hydraulic Engineering **140**, 04014037 (2014).

[6] Craig Hill, Mirko Musa, and Michele Guala, "Interaction between instream axial flow hydrokinetic turbines and uni-directional flow bedforms," Renewable Energy **86**, 409–421 (2016).

[7] Craig Hill, Jessica Kozarek, Fotis Sotiropoulos, and Michele Guala, "Hydrodynamics and sediment transport in a meandering channel with a model axial-flow hydrokinetic turbine," Water Resources Research **52**, 860–879 (2016).

[8] AS Bahaj and LE Myers, "Shaping array design of marine current energy converters through scaled experimental analysis," Energy **59**, 83–94 (2013).

[9] Peter E Robins, Simon P Neill, and Matt J Lewis, "Impact of tidal-stream arrays in relation to the natural variability of sedimentary processes," Renewable Energy **72**, 311–321 (2014).

[10] Peter Bachant and Martin Wosnik, "Performance measurements of cylindrical-and spherical-helical cross-flow marine hydrokinetic turbines, with estimates of exergy efficiency," Renewable

Energy **74**, 318–325 (2015).

[11] Peter Bachant and Martin Wosnik, "Characterising the near-wake of a cross-flow turbine," Journal of Turbulence **16**, 392–410 (2015).

[12] Grégory Pinon, Paul Mycek, Grégory Germain, and Elie Rivoalen, "Numerical simulation of the wake of marine current turbines with a particle method," Renewable Energy **46**, 111–126 (2012).

[13] AS Bahaj, AF Molland, JR Chaplin, and WMJ Batten, "Power and thrust measurements of marine current turbines under various hydrodynamic flow conditions in a cavitation tunnel and a towing tank," Renewable energy **32**, 407–426 (2007).

[14] HNC Breusers and Arved Jaan Raudkivi, *Scouring* (Balkema Rotterdam, The Netherlands, 1991).

[15] Gijsbertus JCM Hoffmans and HJ Verheij, *Scour manual*, Vol. 96 (CRC Press, 1997).

[16] Bruce W Melville and Stephen E Coleman, *Bridge scour* (Water Resources Publication, 2000).

[17] Bruce W Melville, *Local scour at bridge sites*, Ph.D. thesis, School of Engineering, The University of Auckland, Auckland, New Zealand (1975).

[18] Yee Meng Chiew, *Local scour at bridge piers*, Ph.D. thesis, School of Engineering, The University of Auckland, Auckland, New Zealand (1984).

[19] Robert Ettema, *Scour at bridge piers*, Ph.D. thesis, School of Engineering, The University of Auckland, Auckland, New Zealand (1980).

[20] Bruce W Melville, "Pier and abutment scour: integrated approach," Journal of Hydraulic Engineering **123**, 125–136 (1997).

[21] BW Melville and AJ Sutherland, "Design method for local scour at bridge piers," Journal of Hydraulic Engineering **114**, 1210–1226 (1988).

[22] Bruce W Melville and Yee-Meng Chiew, "Time scale for local scour at bridge piers," Journal of Hydraulic Engineering **125**, 59–65 (1999).

[23] Giuseppe Oliveto and Willi H Hager, "Temporal evolution of clear-water pier and abutment scour," Journal of Hydraulic Engineering **128**, 811–820 (2002).

[24] C. Manes and M. Brocchini, "Local scour around structures and the phenomenology of turbulence," J. Fluid Mech. **779**, 309–324 (2015).

[25] G Gioia and FA Bombardelli, "Scaling and similarity in rough channel flows," Physical review letters **88**, 014501 (2001).

[26] Gustavo Gioia and Pinaki Chakraborty, "Turbulent friction in rough pipes and the energy spectrum of the phenomenological theory," Physical review letters **96**, 044502 (2006).

[27] Xiaolei Yang, Ali Khosronejad, and Fotis Sotiropoulos, "Large-eddy simulation of a hydrokinetic turbine mounted on an erodible bed," Renewable Energy **113**, 1419–1433 (2017).

[28] Uriel Frisch, *Turbulence: the legacy of AN Kolmogorov* (Cambridge university press, 1995).

[29] J. Hong, M. Toloui, L.P. Chamorro, M. Guala, and K... Howard, "Natural snowfall reveals large-scale flow structures in the wake of a 2.5-mw wind turbine," Nature communications **5** (2014).

[30] CJ Baker, "The turbulent horseshoe vortex," Journal of Wind Engineering and Industrial Aerodynamics **6**, 9–23 (1980).

[31] Bijan Dargahi, "The turbulent flow field around a circular cylinder," Experiments in Fluids **8**, 1–12 (1989).

[32] Cristian Escauriaza and Fotis Sotiropoulos, "Initial stages of erosion and bed form development in a turbulent flow around a cylindrical pier," Journal of Geophysical Research: Earth Surface **116** (2011).

[33] Cristian Escauriaza and Fotis Sotiropoulos, "Reynolds number effects on the coherent dynamics of the turbulent horseshoe vortex system," Flow, turbulence and combustion **86**, 231–262 (2011).

[34] Tony Burton, David Sharpe, Nick Jenkins, and Ervin Bossanyi, *Wind energy handbook* (John Wiley & Sons, 2001).

[35] KB Howard, JS Hu, LP Chamorro, and M Guala, "Characterizing the response of a wind turbine model under complex inflow conditions," Wind Energy **18**, 729–743 (2015).

[36] K. B. Howard, , and M. Guala, "Upwind preview to a horizontal axis wind turbine: a wind tunnel and field-scale study," Wind Energy **19**, 13711389 (2016).

[37] Albert Shields, *Anwendung der Aehnlichkeitsmechanik und der Turbulenzforschung auf die Geschiebebewegung*, Tech. Rep. (Preussischen Versuchsanstalt für Wasserbau, 1936).

[38] NJ Möller, H Kim, VS Neary, MH García, and LP Chamorro, "On the near-wall effects induced by an axial-flow rotor," Renewable Energy **91**, 524–530 (2016).

[39] Craig Steven Hill, *Interactions Between Channel Topography and Hydrokinetic Turbines: Sediment Transport, Turbine Performance, and Wake Characteristics*, Ph.D. thesis, University of Minnesota (2015).

[40] Mirko Musa, Craig Hill, and Michele Guala, "Local and non-local effects of spanwise finite perturbations in erodible river bathymetries," Bulletin of the American Physical Society **60** (2015).

[41] Giovanni Seminara, Luca Solari, and Gary Parker, "Bed load at low shields stress on arbitrarily sloping beds: Failure of the bagnold hypothesis," Water resources research **38** (2002).

[42] Emmett M Laursen and Arthur Toch, *Scour around bridge piers and abutments*, Vol. 4 (Iowa Highway Research Board Ames, IA, USA, 1956).

[43] R.A. Bagnold, "An approach to the sediment transport problem from general physics," Geological survey professonal paper **422** (1966).

[44] OpenHydro projects, `http://www.openhydro.com/technology.html`, [Accessed on 2 Novermber 2017].

[45] Seokkoo Kang and Fotis Sotiropoulos, "Assessing the predictive capabilities of isotropic, eddy viscosity reynolds-averaged turbulence models in a natural-like meandering channel," Water Resources Research **48** (2012).

[46] A Khosronejad, AT Hansen, JL Kozarek, K Guentzel, M Hondzo, M Guala, P Wilcock, JC Finlay, and F Sotiropoulos, "Large eddy simulation of turbulence and solute transport in a forested headwater stream," Journal of Geophysical Research: Earth Surface **121**, 146–167 (2016).

[47] Ali Khosronejad, Seokkoo Kang, and Fotis Sotiropoulos, "Experimental and computational investigation of local scour around bridge piers," Advances in Water Resources **37**, 73–85 (2012).

[48] Seokkoo Kang, Xiaolei Yang, and Fotis Sotiropoulos, "On the onset of wake meandering for an axial flow turbine in a turbulent open channel flow," Journal of Fluid Mechanics **744**, 376–403 (2014).

[49] Saurabh Chawdhary, Craig Hill, Xiaolei Yang, Michele Guala, Dean Corren, Jonathan Colby, and Fotis Sotiropoulos, "Wake characteristics of a triframe of axial-flow hydrokinetic turbines," Renewable Energy **109**, 332–345 (2017).

[50] Vincent S Neary, Budi Gunawan, Marshall C Richmond, Vibhav Durgesh, Brian Polagye, Jim Thomson, Marian Muste, and Arnie Fontaine, *Field measurements at river and tidal current sites for hydrokinetic energy development: best practices manual*, Tech. Rep. (Oak Ridge National Laboratory (ORNL), 2011).

[51] VS Neary, B Gunawan, and DC Sale, "Turbulent inflow characteristics for hydrokinetic energy conversion in rivers," Renewable and Sustainable Energy Reviews **26**, 437–445 (2013).

[52] Vincent S Neary, Budi Gunawan, Craig Hill, and Leonardo P Chamorro, "Near and far field flow disturbances induced by model hydrokinetic turbine: Adv and adp comparison," Renewable energy **60**, 1–6 (2013).

[53] Jeffrey A Nittrouer, Mead A Allison, and Richard Campanella, "Bedform transport rates for the lowermost mississippi river," Journal of Geophysical Research: Earth Surface **113** (2008).

[54] Daniel Gessler, Brad Hall, Miodrag Spasojevic, Forrest Holly, Hasan Pourtaheri, and Nolan Raphelt, "Application of 3d mobile bed, hydrodynamic model," Journal of Hydraulic Engineering **125**, 737–749 (1999).

[55] B Mutlu Sumer, "Mathematical modelling of scour: A review," Journal of Hydraulic Research **45**, 723–735 (2007).

[56] Sara Bonetti, Gabriele Manoli, Costantino Manes, Amilcare Porporato, and Gabriel G Katul, "Mannings formula and stricklers scaling explained by a co-spectral budget model," Journal of Fluid Mechanics **812**, 1189–1212 (2017).